

# Anomalous High-Energy Waterfall-Like Electronic Structure in $5d$ Transition Metal Oxide $\text{Sr}_2\text{IrO}_4$ with a Strong Spin-Orbit Coupling

Yan Liu<sup>1</sup>, Li Yu<sup>1,\*</sup>, Xiaowen Jia<sup>1</sup>, Jianzhou Zhao<sup>1</sup>, Hongming Weng<sup>1</sup>, Yingying Peng<sup>1</sup>, Chaoyu Chen<sup>1</sup>, Zhuojin Xie<sup>1</sup>, Daixiang Mou<sup>1</sup>, Junfeng He<sup>1</sup>, Xu Liu<sup>1</sup>, Ya Feng<sup>1</sup>, Hemian Yi<sup>1</sup>, Lin Zhao<sup>1</sup>, Guodong Liu<sup>1</sup>, Shaolong He<sup>1</sup>, Xiaoli Dong<sup>1</sup>, Jun Zhang<sup>1</sup>, Zuyan Xu<sup>3</sup>, Chuangtian Chen<sup>3</sup>, Gang Cao<sup>4</sup>, Xi Dai<sup>1</sup>, Zhong Fang<sup>1</sup> and X. J. Zhou<sup>1,2,\*</sup>

<sup>1</sup>*Beijing National Laboratory for Condensed Matter Physics,  
Institute of Physics, Chinese Academy of Sciences, Beijing 100190, China*

<sup>2</sup>*Collaborative Innovation Center of Quantum Matter, Beijing, China*

<sup>3</sup>*Technical Institute of Physics and Chemistry,  
Chinese Academy of Sciences, Beijing 100190, China*

<sup>4</sup>*Department of Physics and Astronomy,  
University of Kentucky, Lexington, KY 40506*

(Dated: January 20, 2015)

The layered  $5d$  transition metal oxides like  $\text{Sr}_2\text{IrO}_4$  have attracted significant interest recently due to a number of exotic and new phenomena induced by the interplay between the spin-orbit coupling, bandwidth  $W$  and on-site Coulomb correlation  $U$ . In contrast to a metallic behavior expected from the Mott-Hubbard model due to more spatially extended  $5d$  orbitals and moderate  $U$ , an insulating ground state has been observed in  $\text{Sr}_2\text{IrO}_4$ . Such an insulating behavior can be understood by an effective  $J_{eff}=1/2$  Mott insulator model by incorporating both electron correlation and strong spin-orbital coupling, although its validity remains under debate at present. In particular,  $\text{Sr}_2\text{IrO}_4$  exhibits a number of similarities to the high temperature cuprate superconductors in the crystal structure, electronic structure, magnetic structure, and even possible high temperature superconductivity that is predicted in doped  $\text{Sr}_2\text{IrO}_4$ . Here we report a new observation of the anomalous high energy electronic structure in  $\text{Sr}_2\text{IrO}_4$ . By taking high-resolution angle-resolved photoemission measurements on  $\text{Sr}_2\text{IrO}_4$  over a wide energy range, we have revealed for the first time that the high energy electronic structures show unusual nearly-vertical bands that extend over a large energy range. Such anomalous high energy behaviors resemble the high energy waterfall features observed in the cuprate superconductors, adding one more important similarity between these two systems. While strong electron correlation plays an important role in producing high energy waterfall features in the cuprate superconductors, the revelation of the high energy anomalies in  $\text{Sr}_2\text{IrO}_4$  points to a novel route in generating exotic electronic excitations from the strong spin-orbit coupling and a moderate electron correlation.

The transition metal oxides exhibit rich exotic physical properties such as high temperature superconductivity and colossal magnetoresistance that have become a central theme of modern condensed matter physics[1, 2]. The insulating ground state of the  $3d$  transition metal oxides can generally be understood by the strong on-site Coulomb repulsion  $U$ , relative to its bandwidth  $W$  ( $U \gg W$ ), as proposed in the Mott-Hubbard model[1]. An insulator-metal transition can occur when  $W \geq U$ . In comparison, in the  $5d$  transition metal oxides, the electron correlation is expected to become less strong due to the more spatially extended  $5d$  orbitals and a metallic ground state is expected[3, 4]. It is thus surprising when it was found that the prototypical  $5d$  compound  $\text{Sr}_2\text{IrO}_4$  is an antiferromagnetic insulator below the Neel

temperature  $T_N \sim 240$  K[5–8]. One popular scenario for the novel insulating ground state of  $\text{Sr}_2\text{IrO}_4$  is the  $J_{eff}=1/2$  Mott insulator model driven by spin-orbit coupling[7]. In this model, five  $5d$  electrons occupy the  $t_{2g}$  orbitals which are split into a fully-filled  $J_{eff}=3/2$  quartet band with lower energy and a half-filled doublet band with  $J_{eff}=1/2$  close to the Fermi level ( $E_F$ ) by strong spin-orbit coupling. Assuming that the width of the  $J_{eff}=1/2$  band is narrow, a moderate Coulomb repulsion  $U$  can open up a gap, giving rise to the so-called  $J_{eff}=1/2$  Mott insulating ground state[7]. While a couple of experimental results are consistent with this scenario[7, 9–17], this picture is challenged due to the fact that the electron hopping energy ( $\sim 0.3$  eV) is not negligible which suggests the  $J_{eff}=1/2$  state alone cannot fully describe the system[18]. Moreover, on the formation mechanism of the insulating ground state in  $\text{Sr}_2\text{IrO}_4$ , an alternative magnetic or Slater-type origin, instead of the Mott-type[7], has been proposed[19] with some experimental support[20–22]. These leave the very nature of the insulating ground state in  $\text{Sr}_2\text{IrO}_4$  open and it is important to study and understand the electronic structure of  $\text{Sr}_2\text{IrO}_4$ .

Angle-resolved photoemission spectroscopy (ARPES) is a powerful tool to directly probe the low energy electronic structures of solid materials[23]. The existing ARPES results on  $\text{Sr}_2\text{IrO}_4$  and related compounds within a relatively narrow energy window appear to agree with the  $J_{eff}=1/2$  model[7, 12–14, 17]. In this paper, we report the observation of unusual high energy bands in  $\text{Sr}_2\text{IrO}_4$ . Our comprehensive angle-resolved photoemission study over a wide energy window reveals for the first time nearly-vertical bands in  $\text{Sr}_2\text{IrO}_4$ . Such exotic bands can not be understood in terms of the band structure calculations; they cannot be understood within the simple  $J_{eff}=1/2$  Mott insulator model or any other existing theoretical models either. The observed high energy anomaly resemble the unusual high energy waterfall bands discovered in the high temperature cuprate superconductors[24–33]. These observations point to the significant role of the strong spin-orbit coupling, together with a moderate electron correlation, in giving rise to new high energy excitations in the  $5d$  transition metal oxides.

The  $\text{Sr}_2\text{IrO}_4$  single crystals were synthesized by flux method[6]. High-resolution angle-resolved photoemission measurements were carried out on our lab system equipped with a Scienta R4000 electron energy analyzer[34]. We use helium discharge lamp as the light source that can provide photon energy of  $h\nu=21.218\text{eV}$  (helium I). The overall energy resolution was set at 20 meV. The angular resolution is  $\sim 0.3$  degree. The Fermi level is referenced

by measuring on a clean polycrystalline gold that is electrically connected to the sample. The sample was cleaved *in situ* and measured at  $\sim 20$  K in ultra-high vacuum with a base pressure better than  $5 \times 10^{-11}$  Torr. The measurements were carried out on different samples for several times and the results are reproducible.

Figure 1 shows the constant energy contours of  $\text{Sr}_2\text{IrO}_4$  at different binding energies. No spectral weight is present at the Fermi level (not shown in Fig. 1), consistent with the insulating nature of  $\text{Sr}_2\text{IrO}_4$ [5–7]. At a binding energy of 0.2 eV, the spectral weight appears first as a circular spot around the  $X(\pi,0)$  and its equivalent locations (Fig. 1a). Further increase of the binding energy to 0.4 eV results in the enlargement of the spot into a square-shape and the emergence of spectral weight near the  $\Gamma(0,0)$  point (Fig. 1b). When the binding energy increases to 0.8 eV, the strong spectral weight near X points vanishes with a formation of a few disconnected patches around X, while the spectral weight near  $\Gamma$  exhibits a petal-like shape with four leaves (Fig. 1c). The measured constant energy contours at low binding energy (0~0.4 eV) are consistent with those reported before[7, 13]. The constant energy contours at an intermediate binding energy (e.g., 0.4 eV) are also consistent with the band structure calculations (Fig. 1d) that include both the on-site Coulomb repulsion  $U$  and the spin-orbit coupling[7]. In terms of the spin-orbit-coupling-driven Mott insulator model[7], the unoccupied states are mainly the  $J_{eff}=1/2$  state, while the occupied states are a mixture of the  $J_{eff}=1/2$  and  $3/2$  states. Due to the strong spin-orbit coupling, the topmost low energy valence state at X is more with  $J_{eff}=1/2$  character ( $\beta$  sheet near X in Fig. 1d), while the topmost low energy valence state at  $\Gamma$  is more with  $J_{eff}=3/2$  character ( $\alpha$  sheet near  $\Gamma$  in Fig. 1d)[7]. The consistency of the low energy electronic structure with the previous reports and the band structure calculations lays a foundation for our following investigation of high binding energy electronic structure in  $\text{Sr}_2\text{IrO}_4$ .

At high binding energies, we find that the electronic structure of  $\text{Sr}_2\text{IrO}_4$  is quite unusual. Figure 2 shows band structure along two high-symmetry momentum cuts covering a large energy range till  $\sim 6$  eV: one cut is across  $\Gamma$  (Fig. 2a-d), the other is across X (Fig. 2e-h). Here we show both the original data (Fig. 2a and 2e), and their corresponding momentum- (Fig. 2b and 2f) and energy-second-derivative (Fig. 2c and 2g) images. The second-derivative images help to highlight the band structure more clearly although many features are already clear in the original data. Since momentum-second derivative image may miss the flat horizontal bands while the energy-second derivative image may miss the vertical

bands, the energy- and momentum-second-derivative images are complementary to each other to provide a full picture. As seen in Fig. 2, at low binding energy (0~1 eV), two prominent bands are observed labeled as  $\alpha_0$  and  $\beta_0$  (Fig. 2c and 2g) that are consistent with the previous reports[7, 13]. However, at higher binding energy, the electronic structure becomes quite unusual. First, the momentum-second derivative images and energy-second-derivative images give rather different band structures for both the  $\Gamma$  and X momentum cuts. Second, as seen in Fig. 2b, a clear vase-shaped band (labeled as  $\alpha_1$  in Fig. 2b) and a vertical waterfall-like band (labeled as  $\alpha_2$  in Fig. 2b) are observed around the  $\Gamma$  point. The vertical band structure is present even beyond 3 eV up to  $\sim 6$  eV (Fig. 2b). Note that these features are not due to the artifact of the momentum second-derivative image because they are already clear in the original data (Fig. 2a). Such features can also be identified clearly in the momentum distribution curves (MDCs) where the peaks corresponding to  $\alpha_1$  and  $\alpha_2$  bands are marked (Fig. 2d). Similar behaviors are observed for the momentum cut across the X point (Fig. 2e) where nearly vertical band structures (labeled as  $\alpha_3$  and  $\beta_1$  in Fig. 2f) are observed up to 4 eV, and another set of vertical bands are seen even up to 6.5 eV (Fig. 2f).

The unusual high energy electronic structure of  $\text{Sr}_2\text{IrO}_4$  is present over a large momentum space. Figure 3 shows the detailed momentum evolution of the high energy electronic structure: one is near the  $\Gamma$  region (Fig. 3a-d) and the other near the X( $0,\pi$ ) region (Fig. 3e-h). While the energy-second-derivative images (Fig. 3d and 3h) show normal two bands ( $\alpha_0$  and  $\beta_0$ ) in the covered energy range as already seen in Fig. 2, nearly vertical bands are observed in the momentum-second-derivative images (Fig. 3c and 3g) in both cases for different momentum cuts. Furthermore, the constant energy contours exhibit dramatic evolution with the binding energy (Fig. 3a and 3e). The spectral weight distribution around the  $\Gamma$  point (Fig. 3a) changes from a pocket centered at  $\Gamma$  at a binding energy of 0.4 eV, to butterfly-shaped at 0.6 eV and 0.8 eV, to big-X-shaped at 1.2 eV and to dumbbell-shaped at 2.0 eV and 2.4 eV. It is interesting to note that the spectral weight distribution shows discrete four strong spots at 0.6 eV and 0.8 eV, other than a continuous contour. From Fig. 3c and 3d, it becomes clear that the drastic spectral distribution change with the binding energy above 1.0 eV is directly related with the presence of the nearly-vertical  $\alpha_1$  and  $\alpha_2$  bands. It is also clear from Fig. 3b that, moving away from the cut across  $\Gamma$  (cut 1), the vase-shaped band and vertical structure persist for the cuts 2 and 3. The same is true for the

X point constant energy contours (Fig. 3e) and the momentum-dependent band structures (Fig. 3f-h). First, the constant energy contours near X also exhibit an obvious evolution with the binding energy (Fig. 3e). Second, the vertical bands are present over a large area of momentum space near X (Fig. 3g).

Figure 4 summarizes the band structure of  $\text{Sr}_2\text{IrO}_4$  measured along three typical high-symmetry momentum cuts (Fig. 4c-e). For comparison, the band structures of  $\text{Sr}_2\text{IrO}_4$  in the antiferromagnetic state are also calculated using the DMFT method with  $U=2.5$ ,  $J=0$  and  $\beta=100$  (Fig. 4a and 4b). In the calculated band structure (Fig. 4a), the electronic states between the Fermi level and 3 eV binding energy are mainly from the Iridium's  $t_{2g}$  orbitals (white lines in Fig. 4a) while above 3 eV binding energy the contribution is mainly from the oxygen p orbitals (yellow lines in Fig. 4a). In addition, the orbital-resolved density of states (DOS) is also calculated where the peak position of  $\alpha_0$  and  $\beta_0$  bands are well resolved (Fig. 4b). In the measured band structure, from the energy-second-derivative image (Fig. 4d), two bands are clearly observed that are marked as  $\alpha_0$  and  $\beta_0$  between  $E_F$  and  $\sim 1$  eV binding energy. These two bands show good agreement with the band structure calculations (Fig. 4a) and previous reports[7, 13]. Also above 3 eV binding energy, the observed bands in the energy-second-derivative image (Fig. 4d) can find some good correspondence in the calculated band structure (Fig. 4a). The most dramatic difference between the measurements and calculations lies in the binding energy region above 1 eV. As seen in Fig. 4a, a couple of energy bands from Iridium are expected from the band structure calculations within the energy range of 1~3 eV but are not observed in the measured data (Fig. 4d). Instead, a number of nearly-vertical band features ( $\alpha_1$ ,  $\alpha_2$ ,  $\alpha_3$  and  $\beta_1$  bands in Fig. 4e) appear within this energy range that are completely absent in the calculated band structure (Fig. 4a). The same is for the 3~6 eV binding energy range where some vertical bands are observed (Fig. 4e) but are not present in the calculated band structure at all (Fig. 4a).

Further inspection of the measured band structure indicates that the new nearly-vertical high energy bands appear to have a close connection with the lower energy  $\alpha_0$  and  $\beta_0$  bands, as shown in Fig. 4c which summarizes all the observed bands on top of the original measured data. One can see that the three vertical bands  $\alpha_1$ ,  $\alpha_2$  and  $\alpha_3$  merge into the  $\alpha_0$  band at lower binding energy while the other vertical band  $\beta_1$  also merges into the lower binding energy  $\beta_0$  band. The low-energy electronic structure of  $\text{Sr}_2\text{IrO}_4$  are mainly composed of  $t_{2g}$

bands that are split into two branches with the effective  $J_{eff}=1/2$  and  $J_{eff}=3/2$  because of the strong spin-orbit coupling[7]. It has been shown that the  $\beta_0$  band is predominantly with the  $J_{eff}=1/2$  character while the  $\alpha_0$  band is mainly with the  $J_{eff}=3/2$  character (Fig. 4a and 4b)[7]. It is interesting to note that one vertical band ( $\beta_1$ ) emerges from the  $J_{eff}=1/2$   $\beta_0$  band while three vertical bands ( $\alpha_1$ ,  $\alpha_2$  and  $\alpha_3$ ) emerge from the  $J_{eff}=3/2$   $\alpha_0$  band (Fig. 4c), consistent with the orbital degeneracy of both the  $J_{eff} = 1/2$  and  $3/2$  bands. These observations indicate the multi-orbital nature of the low energy electronic states in  $\text{Sr}_2\text{IrO}_4$ . In both the  $J_{eff} = 1/2$  and  $3/2$  bands, we have observed such waterfall-like features splitting out of the original bands, this means that the high energy anomaly in  $\text{Sr}_2\text{IrO}_4$  is a general feature appearing for all orbitals over a rather high energy scale.

To the best of our knowledge, such unusual high energy waterfall-like electronic structures are observed for the first time in  $\text{Sr}_2\text{IrO}_4$ . The appearance of nearly-vertical bands is quite unusual because it implies nearly infinite electron velocity if interpreted literally in the conventional band structure picture. This is reminiscent to the high energy waterfall feature observed in the high temperature cuprate superconductors[24–33]. The high energy behaviors are similar between the cuprates and  $\text{Sr}_2\text{IrO}_4$  in a couple of aspects. First, the energy- and momentum-second-derivative images give different band structure[25, 31]. For a conventional metal, the energy- and momentum-second-derivative images are supposed to produce similar band structure. The dichotomy between them already points to an exotic behavior and the effect of strong correlation. Second, nearly vertical bands are observed in the momentum-second-derivative images. The behavior in  $\text{Sr}_2\text{IrO}_4$  is even more dramatic in that several bands show such waterfall-like high energy features (Fig. 4e) while only one band in cuprates shows such a behavior[24–33]. Moreover, the high energy features in  $\text{Sr}_2\text{IrO}_4$  extend over a much larger energy range (1~3 eV for Ir states) (Fig. 4) while it is in the scale of 0.4~1 eV in cuprates[24–33]. The high energy behavior in  $\text{Sr}_2\text{IrO}_4$  is even more complicated, such as the observation of a vase-like shape near the  $\Gamma$  point (  $\alpha_1$  band Fig. 2a and 2b).

The revelation of the high energy waterfall-like bands in  $\text{Sr}_2\text{IrO}_4$  provides another system that can be used to compare and contrast with the cuprates in order to understand the origin of the high energy anomaly. In the cuprate superconductors, the high energy anomalous band has attracted extensive experimental[24–33] and theoretical interest[35–52] although there has been no consensus reached on its origin. The prime candidate for the anomalous high

energy behavior can be simply an intrinsic property of a strong electron correlation system or Mott physics[28, 35, 37, 43–45, 47, 48, 50, 51]. The second possibility is due to quasiparticle scattering with some electronic or bosonic excitations, such as phonons[26], plasmons[38], paramagnons[27, 39, 41, 48], and other spin and charge excitations[52]. It can also be due to other novel effects such as the spin-charge separation[25], spin polarons[36], photoemission matrix element effect[30], charge modulations[40], quantum critical fluctuation[42], in-gap band-tails[46] and so on. Compared with the cuprates where there is a strong electron correlation[2], the electron correlation in *5d* transition metal oxide  $\text{Sr}_2\text{IrO}_4$  is much weaker owing to the much extended *5d* orbitals[7]. On the other hand, due to heavier atomic mass, the spin-orbit coupling becomes an order of magnitude stronger ( $\sim 0.5$  eV)[53] in the *5d* transition metal oxides than that in their *3d* counterparts ( $\sim 20$  meV), reaching a comparable energy scale with the on-site Coulomb repulsion  $U$  and the bandwidth  $W$ [7, 54]. This indicates that the spin-orbit coupling provides a novel tuning parameter in dictating the ground state and physical properties of the *5d* transition metal oxides. While the strong electron correlation plays an important role in producing high energy anomaly in the cuprate superconductors, the observation of the high energy anomaly in  $\text{Sr}_2\text{IrO}_4$  provides a new scenario where the high energy anomaly can be observed in a system with a moderate or weak electron correlation and strong spin-orbit coupling.

One further question comes to whether the moderate electron correlation or the strong spin-orbit coupling alone can produce such a high energy anomaly in  $\text{Sr}_2\text{IrO}_4$  or it is a combined effect. It would be surprising if a moderate electron correlation alone in  $\text{Sr}_2\text{IrO}_4$  can cause the high energy anomaly over much larger energy scale than that in cuprates which has much stronger electron correlation although the possibility cannot be fully ruled out. There is no observation of high energy anomaly reported in systems with dominant spin-orbit coupling like simple metal Bi[55] or topological insulators[56, 57]. The anomalous high energy features can be most likely a combined effect of both the electron correlation and the spin-orbit coupling. This is consistent with the proposition that, in order to understand the insulating behavior of  $\text{Sr}_2\text{IrO}_4$ , both the on-site Coulomb interaction and strong spin-orbit coupling are necessary[7]. It is also consistent with the recent observation of a high energy anomaly in  $\text{UCoGa}_5$  that exhibits a moderate electron correlation and strong spin-orbital coupling[58]. Exotic quasiparticles like a composite particle has been reported lately in  $\text{Sr}_2\text{IrO}_4$ [59]. How the combination of the moderate electron correlation and the strong

spin-orbit coupling can lead to such anomalous high energy excitations in  $\text{Sr}_2\text{IrO}_4$  needs further theoretical and experimental investigations.

Interestingly,  $\text{Sr}_2\text{IrO}_4$  exhibits a number of features that are similar to those of the high temperature cuprate superconductors. First, its crystal structure[5] is similar to that of a parent compound  $\text{La}_2\text{CuO}_4$ [2] with a slight distortion. Second, its insulating nature might be described by a  $J_{eff}=1/2$  Mott insulator model[7] that is similar to the Mott insulator model for the parent compounds of the cuprate superconductors[2]. Third, the electron-doped  $\text{Sr}_2\text{IrO}_4$  shows a single hole-like Fermi surface and Fermi arc[60] that are quite reminiscent to that found in doped cuprate superconductors[23]. It is suggested that the half-filled doublet  $J_{eff}=1/2$  band would be mainly responsible for the low energy insulating physics in  $\text{Sr}_2\text{IrO}_4$  as the role of the half-filled  $d_{x^2-y^2}$  band in cuprate parent compounds. The structural, electronic and magnetic similarities between  $\text{Sr}_2\text{IrO}_4$  and the cuprate parent compound  $\text{La}_2\text{CuO}_4$ [61] imply potential realization of superconductivity in doped  $\text{Sr}_2\text{IrO}_4$ [62]. Our present observation of anomalous high energy waterfall-like feature in  $\text{Sr}_2\text{IrO}_4$  adds one more prominent similarity to that in the cuprate superconductors.

In summary, our ARPES measurements over a wide energy window have revealed for the first time a new phenomenon of the high energy anomalous bands in  $\text{Sr}_2\text{IrO}_4$ . It resembles the high energy waterfall feature observed in high temperature cuprate superconductors. While the low energy electron excitations in  $\text{Sr}_2\text{IrO}_4$  can be described properly by considering both the on-site Coulomb repulsion and the strong spin-orbit coupling[7], the high energy anomalous bands cannot be understood in the framework of the existing band structure calculations. Different from the cuprate superconductors where strong electron correlation plays an important role in producing high energy anomalies, the present results in  $\text{Sr}_2\text{IrO}_4$  provides a new scenario that high energy anomaly can occur in a system with moderate or weak electron correlation and strong spin-orbit coupling. We hope these experimental observations can stimulate further theoretical work in understanding the anomalous electronic behaviors in  $\text{Sr}_2\text{IrO}_4$  in particular, and the high energy anomaly in other materials in general.

\*Corresponding authors: XJZhou@aphy.iphy.ac.cn, li.yu@iphy.ac.cn

---

[1] M. Imada et al., Metal-insulator transitions. Rev. Mod. Phys. **70**, 1039 (1998).

- [2] P. A. Lee et al., Doping a Mott insulator: Physics of high-temperature superconductivity. *Rev. Mod. Phys.* **78**, 17 (2006).
- [3] L. F. Mattheiss, Band structure and Fermi surface of  $\text{ReO}_3$ . *Phys. Rev.* **181**, 987 (1969).
- [4] L. F. Mattheiss, Electronic structure of  $\text{RuO}_2$ ,  $\text{OsO}_2$ , and  $\text{IrO}_2$ . *Phys. Rev. B* **13**, 2433 (1976).
- [5] M. K. Crawford et al., Structural and magnetic studies of  $\text{Sr}_2\text{IrO}_4$ . *Phys. Rev. B* **49**, 9198 (1994).
- [6] G. Cao et al., Weak ferromagnetism, metal-to-nonmetal transition, and negative differential resistivity in single-crystal  $\text{Sr}_2\text{IrO}_4$ . *Phys. Rev. B* **57**, 11039(R) (1998).
- [7] B. J. Kim et al., Novel  $J_{eff}=1/2$  Mott state induced by relativistic spin-orbit coupling in  $\text{Sr}_2\text{IrO}_4$ . *Phys. Rev. Lett.* **101**, 076402 (2008).
- [8] S. Fujiyama et al., Two-dimensional Heisenberg behavior of  $J_{eff}=1/2$  isospins in the paramagnetic state of the spin-orbital Mott insulator  $\text{Sr}_2\text{IrO}_4$ . *Phys. Rev. Lett.* **108**, 247212 (2012).
- [9] S. J. Moon et al., Dimensionality-controlled insulator-metal transition and correlated metallic state in 5d transition metal oxides  $\text{Sr}_{n+1}\text{Ir}_n\text{O}_{3n+1}$  ( $n=1, 2$ , and  $\infty$ ). *Phys. Rev. Lett.* **101**, 226402 (2008).
- [10] B. J. Kim et al., Phase-sensitive observation of a spin-orbital Mott state in  $\text{Sr}_2\text{IrO}_4$ , *Science* **323**, 1329 (2009).
- [11] K. Ishill et al., Momentum-resolved electronic excitations in the Mott insulator  $\text{Sr}_2\text{IrO}_4$  studied by resonant inelastic x-ray scattering. *Phys. Rev. B.* **83**, 115121 (2011).
- [12] B. M. Wojek et al., The  $J_{eff}=1/2$  insulator  $\text{Sr}_3\text{Ir}_2\text{O}_7$  studied by means of angle-resolved photoemission spectroscopy. *J. Phys. Con. Matt.* **24**, 415602 (2012).
- [13] Q. Wang et al., Dimensionality-controlled Mott transition and correlation effects in single-layer and bilayer perovskite iridates. *Phys. Rev. B.* **87**, 245109 (2013).
- [14] S. Moser et al., The electronic structure of the high-symmetry perovskite iridate  $\text{Ba}_2\text{IrO}_4$ . *New J. Phys.* **16**, 013008 (2014).
- [15] J. Nichols et al., Tunneling into the Mott insulator  $\text{Sr}_2\text{IrO}_4$ . *Phys. Rev. B* **89**, 085125 (2014).
- [16] J. X. Dai et al., Local density of states study of a spin-orbit-coupling induced Mott insulator  $\text{Sr}_2\text{IrO}_4$ . *Phys. Rev. B.* **90**, 041102(R) (2014).
- [17] Y. Cao et al., Hallmarks of the Mott-Metal crossover in the hole doped  $J=1/2$  Mott insulator  $\text{Sr}_2\text{IrO}_4$ . *arXiv:1406.4978* (2014).
- [18] H. Watanabe et al., Microscopic study of a spin-orbit-induced Mott insulator in Ir oxides.

- Phys. Rev. Lett. **105**, 216410 (2010).
- [19] R. Arita et al., Ab initio studies on the interplay between spin-orbit interaction and Coulomb correlation in  $\text{Sr}_2\text{IrO}_4$  and  $\text{Ba}_2\text{IrO}_4$ . Phys. Rev. Lett. **108**, 086403 (2012).
- [20] D. Hsieh et al., Observation of a metal-to-insulator transition with both Mott-Hubbard and Slater characteristics in  $\text{Sr}_2\text{IrO}_4$  from time-resolved photocarrier dynamics. Phys. Rev. B. **86**, 035128 (2012).
- [21] A. Yamasaki et al., Bulk nature of layered perovskite Iridates beyond the Mott scenario: An approach from bulk sensitive photoemission study. Phys. Rev. B. **89**, 121111(R) (2014).
- [22] Q. Li et al., Atomically resolved spectroscopic study of  $\text{Sr}_2\text{IrO}_4$ : Experiment and theory. Scientific reports **3**, 3073 (2013).
- [23] A. Damascelli et al., Angle-resolved photoemission studies of the cuprate superconductors. Rev. Mod. Phys. **75**, 473 (2003).
- [24] F. Ronning et al., Anomalous high-energy dispersion in angle-resolved photoemission spectra from the insulating cuprate  $\text{Ca}_2\text{CuO}_2\text{Cl}_2$ . Phys. Rev. B **71**, 094518 (2005).
- [25] J. Graf et al., Universal High Energy Anomaly in the Angle-Resolved Photoemission Spectra of High Temperature Superconductors: Possible Evidence of Spinon and Holon Branches. Phys. Rev. Lett. **98**, 067004 (2007).
- [26] B. P. Xie et al., High-Energy Scale Revival and Giant Kink in the Dispersion of a Cuprate Superconductor. Phys. Rev. Lett. **98**, 147001 (2007).
- [27] T. Valla et al., High-Energy Kink Observed in the Electron Dispersion of High-Temperature Cuprate Superconductors. Phys. Rev. Lett. **98**, 167003 (2007).
- [28] W. Meevasana et al., Hierarchy of multiple many-body interaction scales in high-temperature superconductors. Phys. Rev. B **75**, 174506 (2007).
- [29] J. Chang et al., When low- and high-energy electronic responses meet in cuprate superconductors. Phys. Rev. B **75**, 224508 (2007).
- [30] D. S. Inosov et al., Momentum and Energy Dependence of the Anomalous High-Energy Dispersion in the Electronic Structure of High Temperature Superconductors. Phys. Rev. Lett. **99**, 237002 (2007).
- [31] W. Zhang et al., High Energy Dispersion Relations for the High Temperature  $\text{Bi}_2\text{Sr}_2\text{CaCu}_2\text{O}_8$  Superconductor from Laser-Based Angle-Resolved Photoemission Spectroscopy. Phys. Rev. Lett. **101**, 017002 (2008).

- [32] B. Moritz et al., Effect of strong correlations on the high energy anomaly in hole- and electron-doped high- $T_c$  superconductors. *New J. Phys.* **11**, 093020 (2009).
- [33] M. Ikeda et al., Differences in the high-energy kink between hole- and electron-doped high- $T_c$  superconductors. *Phys. Rev. B* **80**, 184506 (2009).
- [34] G. D. Liu et al., Development of a vacuum ultraviolet laser-based angle-resolved photoemission system with a superhigh energy resolution better than 1 meV. *Rev. Sci. Instrum.* **79**, 023105 (2008).
- [35] K. Byczuk et al., Kinks in the dispersion of strongly correlated electrons. *Nature Phys.* **3**, 168(2007).
- [36] E. Manousakis, String excitations of a hole in a quantum antiferromagnet and photoelectron spectroscopy. *Phys. Rev. B* **75**, 035106(2007).
- [37] R. G. Leigh et al., Hidden Charge  $2e$  Boson in Doped Mott Insulators. *Phys. Rev. Lett.* **99**, 046404 (2007).
- [38] R. S. Markiewicz and A. Bansil, Dispersion anomalies induced by the low-energy plasmon in the cuprates. *Phys. Rev. B* **75**, 020508(R)(2007).
- [39] R. S. Markiewicz, S. Sahrakorpi and A. Bansil, Paramagnon-induced dispersion anomalies in the cuprates. *Phys. Rev. B* **76**, 174514 (2007).
- [40] T. Zhou and Z. D. Wang, High-energy dispersion anomaly induced by the charge modulation in high- $T_c$  superconductors. *Phys. Rev. B* **75**, 184506 (2007).
- [41] A. Macridin et al., High-Energy Kink in the Single-Particle Spectra of the Two-Dimensional Hubbard Model. *Phys. Rev. Lett.* **99**, 237001(2007).
- [42] L. Zhu et al., Universality of Single-Particle Spectra of Cuprate Superconductors. *Phys. Rev. Lett.* **100**, 057001(2008).
- [43] F. Tan et al., Theory of high-energy features in single-particle spectra of hole-doped cuprates. *Phys. Rev. B* **76**, 054505(2007).
- [44] M. M. Zempljic et al., Temperature and Doping Dependence of the High-Energy Kink in Cuprates. *Phys. Rev. Lett.* **100**, 036402 (2008).
- [45] P. Srivastava et al., High-energy kink in the dispersion of a hole in an antiferromagnet: Double-occupancy effects on electronic excitations. *Phys. Rev. B.* **76**, 184435 (2007).
- [46] A. S. Alexandrov and K. Reynolds, Angle-resolved photoemission spectroscopy of band tails in lightly doped cuprates. *Phys. Rev. B* **76**, 132506(2007).

- [47] C. Weber, K. Haule and G. Kotliar, Optical weights and waterfalls in doped charge-transfer insulators: A local density approximation and dynamical mean-field theory study of  $\text{La}_{2-x}\text{Sr}_x\text{CuO}_4$ . *Phys. Rev. B* **78**, 134519 (2008)
- [48] S. Basak et al., Origin of the high-energy kink in the photoemission spectrum of the high-temperature superconductor  $\text{Bi}_2\text{Sr}_2\text{CaCu}_2\text{O}_8$ , *Phys. Rev. B* **80**, 214520 (2009).
- [49] S. Sakai, Y. Motome and M. Imada, Doped high-Tc cuprate superconductors elucidated in the light of zeros and poles of the electronic Greens function, *Phys. Rev. B* **82**, 134505 (2010).
- [50] D. Katagiri et al., Theory of the waterfall phenomenon in cuprate superconductors. *Phys. Rev. B* **83**, 165124 (2011).
- [51] B. D. Piazza et al., Unified one-band Hubbard model for magnetic and electronic spectra of the parent compounds of cuprate superconductors. *Phys. Rev. B* **85**, 100508(R) (2012).
- [52] G. Mazza et al., Evidence for phonon-like charge and spin fluctuations from an analysis of angle-resolved photoemission spectra of  $\text{La}_{2-x}\text{Sr}_x\text{CuO}_4$  superconductors. *Phys. Rev. B* **87**, 014511 (2013).
- [53] M. Montalti et al., *Handbook of Photochemistry*, Third Edition (2006).
- [54] M. Ge et al., Lattice-driven magnetoresistivity and metal-insulator transition in single-layered iridates. *Phys. Rev. Lett.* **84**, 100402(R) (2011).
- [55] P. Hofmann, The surfaces of bismuth: Structural and electronic properties. *Progress in Surface Science* **81**, 191 (2006).
- [56] M. Hasan and C. Kane, Colloquium: Topological insulators. *Rev. Mod. Phys.* **82**, 3045 (2010).
- [57] X. L. Qi and S. C. Zhang, Topological insulators and superconductors. *Rev. Mod. Phys.* **83**, 1057 (2011).
- [58] T. Das et al., *Phys. Rev. X* **2** 041012 (2012).
- [59] J. Kim et al., Excitonic quasiparticles in a spin-orbit Mott insulator. *Nature Communications* **5**, 4453 (2014).
- [60] Y. K. Kim et al., Fermi arcs in a doped pseudospin-1/2 Heisenberg antiferromagnet. *Science* **345**, 6193(2014).
- [61] F. Wang et al., Twisted Hubbard model for  $\text{Sr}_2\text{IrO}_4$ : Magnetism and possible high temperature superconductivity. *Phys. Rev. Lett.* **106**, 136402 (2011).
- [62] H. Watanabe et al., Monte Carlo study of an unconventional superconducting phase in Iridium oxide  $J_{eff}=1/2$  Mott insulators induced by carrier doping. *Phys. Rev. Lett.* **110**, 027002

(2013).

**Acknowledgement** XJZ thanks financial support from the NSFC (91021006 and 11334010), the MOST of China (973 program No: 2011CB921703, 2011CBA00110, 2012CB821402, 2013CB921700 and 2013CB921904), and the Strategic Priority Research Program (B) of the Chinese Academy of Sciences (Grant No. XDB07020300).

### **Author Contributions**

X.J.Z. and Y.L. proposed and designed the research. G.C. contributed in sample preparation. Y.L., L.Y., X.W.J., Y.Y.P., C.Y.C., Z.J.X., D.X.M., J.F.H., X.L., Y.F., H.M.Y., L.Z., G.D.L., S.L.H., X.L.D., J.Z., Z.Y.X., C.T.C. and X.J.Z. contributed to the development and maintenance of Laser-ARPES system. Y.L. carried out the ARPES experiment. Y.F., L.Y. and X.J.Z. analyzed the data. J.Z.Z., H.M.W., X.D. and Z.F. performed band structure calculations. X.J.Z., Y.L. and L.Y. wrote the paper and all authors participated in discussion and comment on the paper.

### **Additional information**

**Competing financial interests:** The authors declare no competing financial interests.

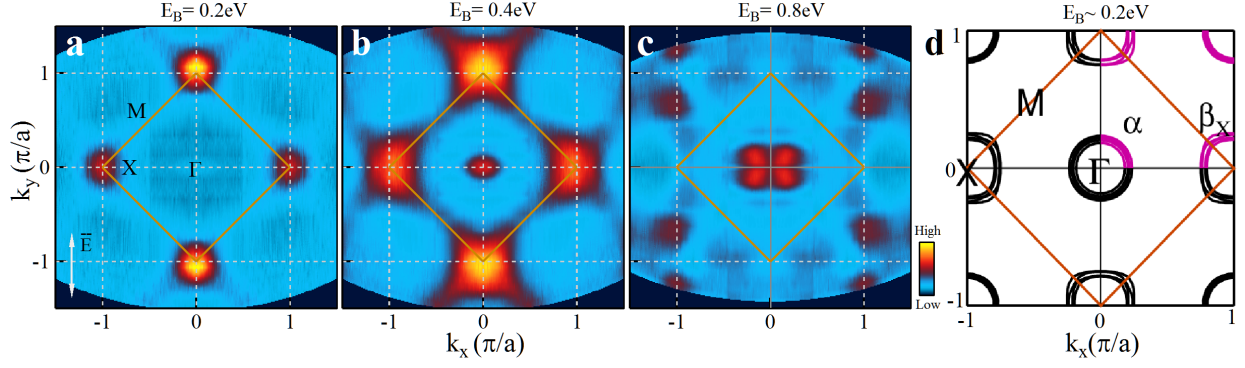


FIG. 1: Measured constant energy contours of  $\text{Sr}_2\text{IrO}_4$  and its comparison with calculations. (a-c) represent constant energy contours of the spectral weight distribution for  $\text{Sr}_2\text{IrO}_4$  measured at  $\sim 20 \text{ K}$  at different binding energies ( $E_B$ ) of  $0.2 \text{ eV}$ ,  $0.4 \text{ eV}$ , and  $0.8 \text{ eV}$ , respectively. (d) is the calculated constant energy contour at a binding energy of  $\sim 0.2 \text{ eV}$  by including on-site Coulomb repulsion and spin-orbit coupling[7]. The orange lines denote the antiferromagnetic Brillouin zone boundary for the  $\text{IrO}_2$  plane.

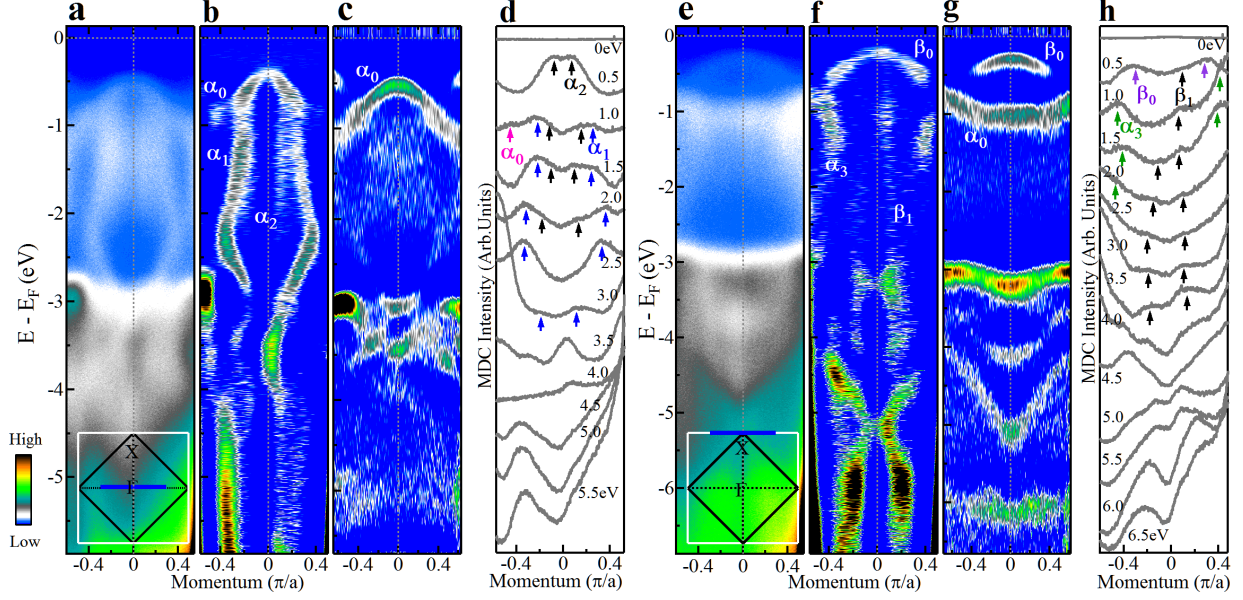


FIG. 2: **Typical band structures of  $\text{Sr}_2\text{IrO}_4$  along high-symmetry cuts in a large energy range.** (a) Original photoemission image of  $\text{Sr}_2\text{IrO}_4$  measured along a high-symmetry cut across  $\Gamma$ ; the location of the cut is shown as a solid blue line in the inset. (b) and (c) are corresponding momentum-second-derivative and energy-second-derivative images of (a), respectively. (d) Momentum distribution curves (MDCs) at different binding energies obtained from (a). (e). Original photoemission image measured along a high-symmetry cut across X; the location of the cut is shown as a solid blue line in the inset. (f) and (g) are corresponding momentum-second-derivative and energy-second-derivative images of (e), respectively. (h) MDCs at different binding energies obtained from (e).

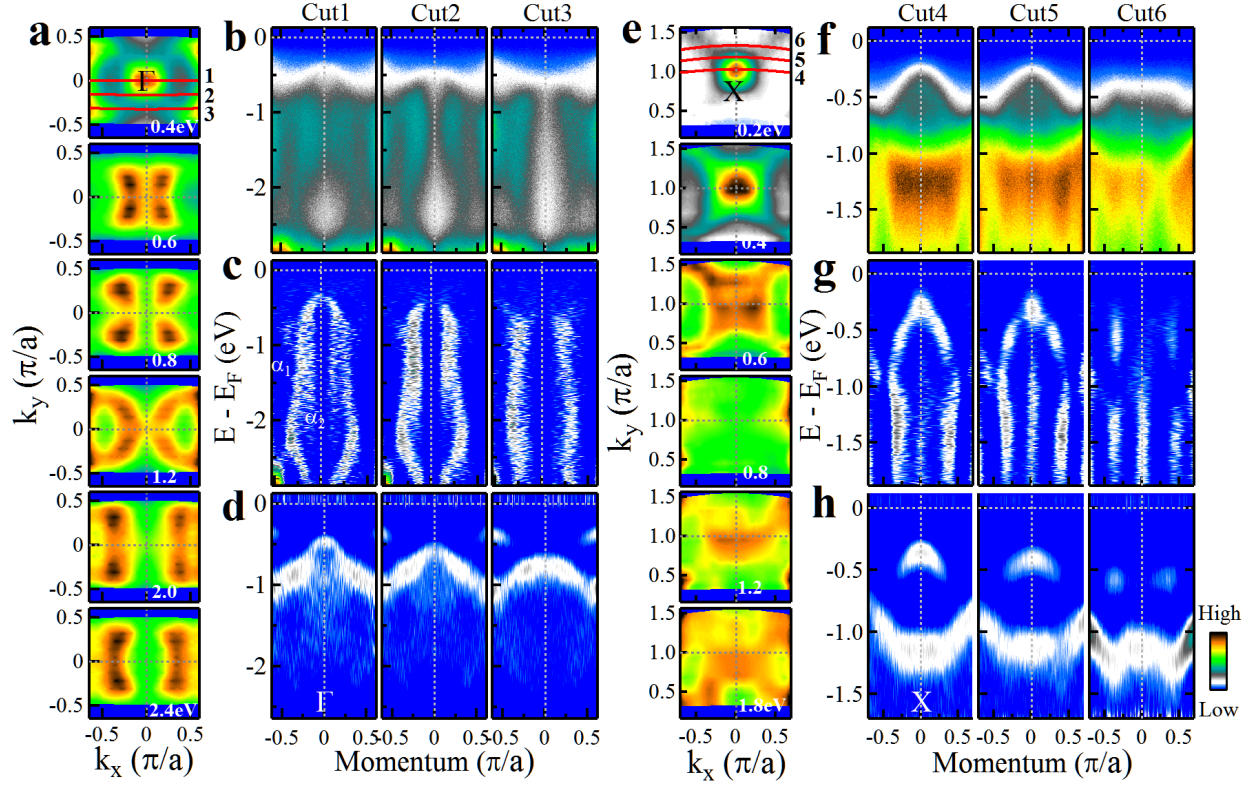


FIG. 3: Momentum dependence of the band structures around  $\Gamma$  and X regions. (a) Constant energy contours around  $\Gamma$  point at different binding energies from 0.4 eV (top panel) to 0.6, 0.8, 1.2, 2.0 and 2.4 eV (bottom panel). (b) Original photoemission images measured along different momentum cuts around  $\Gamma$ . The location of the momentum cuts are shown as red lines in the top panel of (a). (c) and (d) are corresponding momentum-second-derivative and energy-second-derivative images of (b), respectively. (e) Constant energy contours around X point at different binding energies from 0.2 eV (top panel) to 0.4, 0.6, 0.8, 1.2 and 1.8 eV (bottom panel). (f) Original photoemission images measured along different momentum cuts around X. The location of the momentum cuts are shown as red lines in the top panel of (e). (g) and (h) are corresponding momentum-second-derivative and energy-second-derivative images of (f), respectively.

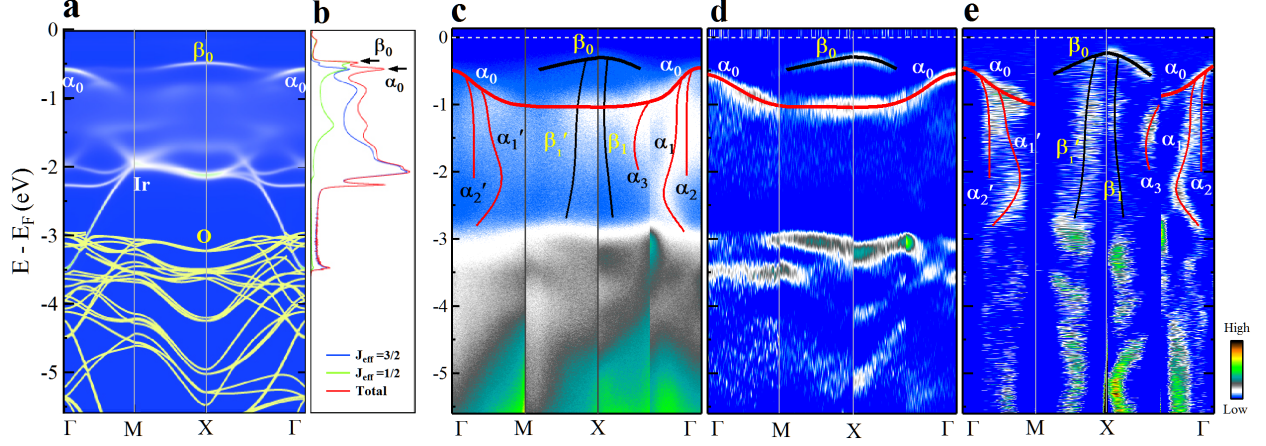


FIG. 4: **Calculated and measured overall band structure of  $\text{Sr}_2\text{IrO}_4$ .** (a) Band structure of  $\text{Sr}_2\text{IrO}_4$  by DMFT calculations along high symmetry line in the first Brillouin zone. The white lines are the LDA+DMFT calculation on Iridium's  $t_{2g}$  orbitals while the yellow lines are the LDA calculation on Oxygen p orbitals. (b) Calculated density-of-states for the  $J_{\text{eff}}=3/2$  and  $J_{\text{eff}}=1/2$  states, and the total density-of-states of the Iridium orbitals. (c). Overall measured original photoemission image of  $\text{Sr}_2\text{IrO}_4$  along high-symmetry cuts. The observed bands are overlaid on top of the original data. (d) and (e) are corresponding energy-second-derivative and momentum-second-derivative images of (c), respectively. The black and red lines are guides to the eye for the bands that can be resolved.  $\alpha'_1$ ,  $\alpha'_2$  and  $\beta'_1$  bands are equivalent bands to the  $\alpha_1$ ,  $\alpha_2$ , and  $\beta_1$  bands along other symmetry cuts.